

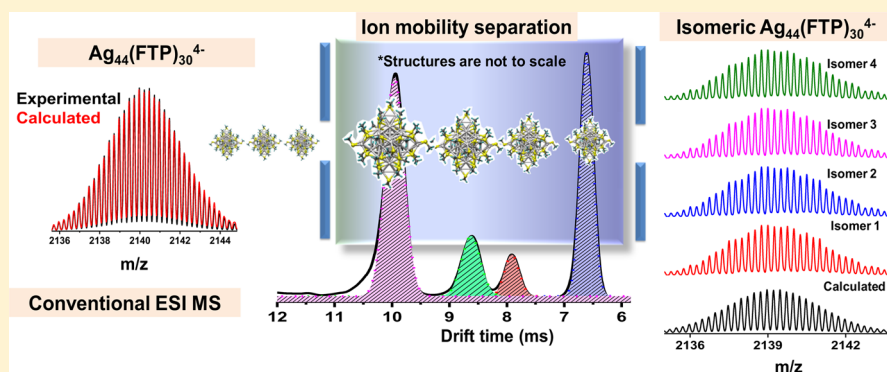
Isomerism in Monolayer Protected Silver Cluster Ions: An Ion Mobility-Mass Spectrometry Approach

Ananya Bakshi,^{†,§} Atanu Ghosh,^{†,§} Sathish Kumar Mudedla,[‡] Papri Chakraborty,[†] Shridevi Bhat,[†] Biswajit Mondal,[†] K. R. Krishnadas,[†] Venkatesan Subramanian,[‡] and Thalappil Pradeep^{*,†,§}

[†]Department of Chemistry, Indian Institute of Technology, Madras, Chennai 600036, India

[‡]Chemical Laboratory, CSIR-Central Leather Research Institute, Adyar, Chennai 600020, India

S Supporting Information



ABSTRACT: Experimental evidence for the existence of gas phase isomers in monolayer protected noble metal clusters is presented, taking $\text{Ag}_{44}(\text{SR})_{30}$ (SR = 4-fluorothiophenol, *p*-mercaptobenzoic acid) and $\text{Ag}_{29}(\text{BDT})_{12}$ (BDT: benzene dithiol) clusters as examples which do not show any isomeric structures in their crystals. Electrospray ionization coupled with ion mobility separation allowed for the identification of multiple isomers of $\text{Ag}_{44}\text{SR}_{30}$ cluster in its 3- and 4- charge states, their most abundant gas phase ions. $\text{Ag}_{29}(\text{BDT})_{12}$ showed isomerism in its common 3- charge state. Isomerism is likely to be due to different types of ligand orientations in the staples leading to changes in the overall size and shape of the cluster ions, which was further confirmed by density functional theory calculations on $\text{Ag}_{44}(\text{FTP})_{30}^{4-}$. No isomers were seen in the ions of the well-known cluster, $\text{Au}_{25}\text{SR}_{18}$ (SR = phenylethanethiol, dodecanethiol, and butanethiol).

1. INTRODUCTION

Atomically precise clusters of noble metals protected with ligands or aspicules (shielded molecules)¹ have evolved into a family of new materials with novel properties.² Along with their structural diversity, novel phenomena and related applications have resulted in an explosion of activities. While their solution phase properties probed by spectroscopic methods attracted significant attention, phenomena in the gas phase have not been investigated to the same extent. Difficulties associated with the formation of intact gas phase species and exploring them at high resolution have been the limiting factors in such studies. Recent advances in ion formation and mass analysis at high resolution coupled with ion mobility (IM) separation can provide newer insights into the gas phase properties of such systems. Ion mobility technique is used extensively to understand protein conformers in the gas phase.^{3–5} Mobility of any ion depends mainly on three factors: mass to charge ratio (m/z), size, and shape. Structural or conformational isomers have the same m/z , which makes it difficult to identify those isomers using conventional mass spectrometric analyses. On the other hand, mass spectrum coupled with IM allows their separation according to their drift time (time taken to

travel through the drift tube or ion mobility cell). This property gives a third dimension to the mass spectrum.

In this manuscript, we present the first detailed experimental observation of the existence of gas phase isomers in aspicules, by ion mobility mass spectrometry (IM MS) which does not show any isomers in their condensed phase. Although IM separation is often practiced in macromolecular studies to understand conformations and specific interactions with other molecules, it is not yet common in materials science. Very few reports exist on IM MS analysis of monolayer-protected clusters.^{6–10} In a recent report, isomers of the $\text{Ag}_{11}(\text{SG})_7^{3-}$ cluster ion was identified by ion mobility mass spectrometry.¹⁰ However, as no glutathione protected cluster has been crystallized so far, we do not have any information on the absence of isomers in the condensed phase for such clusters. The clusters discussed in the current manuscript are all crystallized, and none of them show isomerism in their condensed phase.

Received: May 11, 2017

Published: June 1, 2017

2. EXPERIMENTAL SECTION

2.1. Materials and Methods. **2.1.1. Materials.** Silver nitrate (AgNO_3), dichloromethane (DCM), phenylethanethiol (PET), 4-fluorothiophenol, *p*-MBA, methanol (MeOH), benzene dithiol (BDT), and sodium borohydride (NaBH_4) were purchased from Sigma-Aldrich. Chloroauric acid ($\text{HAuCl}_4 \cdot 3\text{H}_2\text{O}$) was prepared in laboratory from pure gold. All of the chemicals were used without further purification.

2.1.1.1. Synthesis of $\text{Na}_4\text{Ag}_{44}(\text{p-MBA})_{30}$. About 128 mg of AgNO_3 was added to a mixture of DMSO and water (4:7 volume ratio) in a beaker, and 173 mg of MBA was added to the mixture and stirred continuously for the formation of silver thiolates. Formation of thiolates was confirmed by the turbidity of the solution. To this, around 50% CsOH was added dropwise until the turbidity disappeared and a clear greenish yellow solution was obtained. To reduce the thiolates to the desired clusters, ice-cold NaBH_4 solution (283 mg in 9 mL water) was added dropwise. Within 1 h, the color slowly changed from deep brown to deep red confirming the formation of $\text{Na}_4\text{Ag}_{44}(\text{p-MBA})_{30}$ clusters. The as-synthesized clusters were precipitated using excess DMF and centrifuged. The precipitate was redissolved in DMF containing citric acid. Citric acid acidifies the carboxylic acid groups of *p*-MBA so that the cluster can be soluble in DMF. To avoid any impurities, the clusters were again precipitated using toluene and centrifuged followed by acidification by citric acid. The purified clusters were redissolved in DMF and was used for further study.

2.1.1.2. Synthesis of $[\text{PPh}_4]_4\text{Ag}_{44}(\text{FTP})_{30}$. The clusters were synthesized following a solid state synthesis route where 20 mg of AgNO_3 and 12 mg of PPh_4Br were ground together in an agate mortar and pestle. To the mixture was added 76 μL of 4-FTP and ground again to get silver thiolates which were reduced to clusters by the addition of 45 mg of dry NaBH_4 . The formation of a brown colored mixture indicated successful reduction of the thiolates to clusters. The resulting mixture was immediately extracted with 7 mL of DCM and kept undisturbed at room temperature and monitored using UV-vis absorption spectroscopy until the appearance of all characteristic absorption features of the clusters. The clusters were purified following the above-mentioned method for $\text{Na}_4\text{Ag}_{44}(\text{p-MBA})_{30}$ and the solution was rotavapored to obtain a powder sample. The powder was dissolved in different solvents for further studies.

2.1.1.3. Synthesis of $\text{Ag}_{29}(\text{BDT})_{12}$. $\text{Ag}_{29}(\text{BDT})_{12}$ clusters were synthesized following the reported method.¹⁸ About 20 mg of AgNO_3 was dissolved in a 15 mL mixture of 1:2 MeOH/DCM. To this solution was added 13.5 μL of BDT which resulted in turbid yellow solution indicating the formation of insoluble silver thiolates. To this was added 200 mg of PPh_3 dissolved in 1 mL of DCM to get a colorless solution. The reaction mixture was kept under stirring, and a freshly prepared ice-cold solution of 10.5 mg of NaBH_4 in 500 μL of water was added after 15 min. The initial dark brown color of the solution gradually turned to orange over time. The reaction mixture was stirred in dark for another 3 h. After the completion of the reaction, the solution mixture was centrifuged and the supernatant was discarded. The precipitate consisting of the $\text{Ag}_{29}(\text{BDT})_{12}$ cluster was washed repeatedly with ethanol to remove all of the unreacted species. The purified cluster was used for further studies.

2.1.2. Instrumental Details. All of the mass spectrometric experiments described in this work were carried out in Waters'

Synapt G2Si HDMS instrument equipped with an electrospray source, quadrupole ion guide/trap, ion mobility cell, and TOF detector. The instrument can also operate in matrix assisted laser desorption ionization (MALDI) and atmospheric pressure chemical ionization (APCI) mode. We have used only the ESI mode for our present study. All ion mobility data presented here were performed with high pure nitrogen in the ion mobility drift tube. As all of the clusters possess inherent negative charge in the core and detected in negative ion mode, the experiments were done only in negative ion ESI mode. About 1 $\mu\text{g}/\text{mL}$ $\text{Ag}_{44}(\text{FTP})_{30}$ cluster solution was prepared in DCM and directly infused with a flow rate of 10 $\mu\text{L}/\text{min}$. Minimum capillary voltage applied to get a well resolved mass spectrum was 100 V. Cone voltage and source offset were kept at 0 V to avoid any in-source fragmentation. For ion mobility experiments, bias voltage was kept at 45 V for 3- charged species and the spectra were collected in the mass range of m/z 2000–4000. To get well separated isomeric peaks, the mass range was reduced to m/z 2700–3000. Wave velocity was optimized at 650 m/s and a height of 40 V was used in the mobility cell. The helium and nitrogen gas flow rates were set to 150 and 90 mL/min, respectively. For the 4- charged species, bias voltage was kept at 27 V and all other parameters were kept the same as described for 3- charged species. To obtain $\text{Ag}_{44}(\text{FTP})_{30}$ mass spectrum in ion mobility (ESI IM-MS) mode, the following instrumental parameters were used: sample concentration: 1 $\mu\text{g}/\text{mL}$; solvent: DCM; flow rate: 10–20 $\mu\text{L}/\text{min}$; capillary voltage: 100–500 V; cone voltage: 0–20 V; source offset: 0–10 V; desolvation gas flow: 400 L/h; trap gas flow: 2 mL/min; He gas flow: 100 mL/min; ion mobility gas flow: 50 mL/min; bias voltage: 27–45 V; wave velocity: 400–650 m/s; wave height: 30–40 V; UV-vis absorption studies were conducted with a PerkinElmer Lambda25 instrument with 1 nm band-pass.

3. RESULTS AND DISCUSSION

For this study, we have considered four celebrated clusters of Au and Ag for which crystal structures are known; namely, $\text{Ag}_{44}(\text{SR})_{30}$,^{11–14} $\text{Ag}_{25}(\text{SR})_{18}$,¹⁵ $\text{Au}_{25}(\text{SR})_{18}$,^{16,17} and $\text{Ag}_{29}(\text{BDT})_{12}$.¹⁸ They were prepared by established methods (details of synthesis, characterization, and essential data are in the Supporting Information, SI). Clusters in the solid state are often charged and exist with counterions such as Na^+ (see the SI), although in our discussion, only the molecular species is mentioned. In certain cases such as $\text{Ag}_{29}(\text{BDT})_{12}$, there is also a secondary coordination shell involving phosphines, which makes its overall formula $\text{Ag}_{29}(\text{BDT})_{12}(\text{PPh}_3)_4$. Their unique optical absorption and mass spectral features allow them to be characterized completely. $\text{Au}_{25}(\text{SR})_{18}$ is composed of a 13 atom icosahedral core, protected with 6 $\text{Au}_2(\text{SR})_3$ staple motifs.^{1,16} The recently reported $\text{Ag}_{25}(\text{SR})_{18}$ ¹⁵ resembles $\text{Au}_{25}(\text{SR})_{18}$ closely, as confirmed from the crystal structure. Unlike these similarly structured clusters, $\text{Ag}_{44}(\text{SR})_{30}$ possesses a completely different type of core arrangement.^{11–14} This cluster is a hollow cage cluster as the atom at the center of the first icosahedron is missing. This unique structure is responsible for the characteristic absorption features and different optical properties of the cluster.

Three different ligand protected $\text{Ag}_{44}(\text{SR})_{30}$ clusters were investigated in this study. The ligands are 4-fluorothiophenol (FTP), *p*-mercaptobenzoic acid (*p*-MBA), and difluorothiophenol (DFTP; see the SI for their synthesis and essential characterization; Figure S1 and S2). A Waters Synapt G2Si

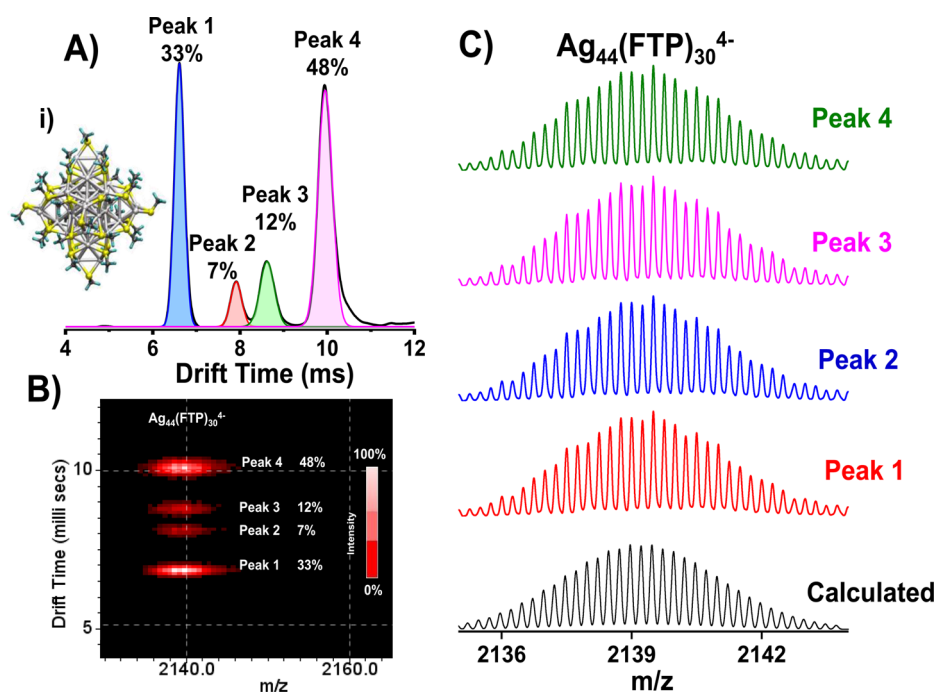


Figure 1. (A) Drift time profile of $\text{Ag}_{44}(\text{FTP})_{30}^{4-}$ (m/z 2140) showing four peaks due to distinct isomeric structures with relative abundances of 33, 7, 12, and 48%, respectively (calculated from peak area). Calculated structure of $\text{Ag}_{44}(\text{SMe})_{30}$ is shown in inset (i). (B) Four well-defined spots observed in m/z vs drift time plot. Each spot gave the same mass spectrum as shown in C, matched with the spectrum.

HDMS mass spectrometer equipped with an electrospray ionization (ESI) source coupled with an IM separation cell was used which allows simultaneous monitoring of ions by MS with or without IM (see the [Experimental Section](#) for instrument details). The cluster $[\text{Ag}_{44}(\text{FTP})_{30}]$ shows the 4^- ion (m/z 2140) as the major peak along with the 3^- (m/z 2853) and the 2^- (m/z 4283) ions, when analyzed in negative ion mode. An expanded mass spectrum of $[\text{Ag}_{44}(\text{FTP})_{30}]^{4-}$ is shown in [Figure 1](#) showing the characteristic isotope pattern. The mass spectrum fits exactly with the calculated spectrum with the isotope peaks resolved perfectly ([Figures 1C](#) and [S1](#)). When the mass selected ions (m/z 2140) were passed through the IM cell, four well-separated spots were observed in the mobilogram (m/z vs ion mobility drift time plot). All of these spots were converted to respective drift times. Relative abundances of each species were calculated from the area under the curve. Two major peaks (peaks 1 and 4 in [Figure 1B](#)) were observed at 6.5 and 9.8 ms with 33 and 48% relative abundances, respectively. Two low intensity peaks (labeled 3 and 4) were also observed at 7.9 and 8.5 ms with 7 and 12% relative abundances. All of these features show identical masses as shown in the inset implying that they are due to isomers. All of the experiments were performed at the lowest capillary voltage to avoid any possible structural distortion of the intact molecule in the gas phase as a result of applied potential. $\text{Ag}_{44}(\text{FTP})_{30}$ is a highly ionizable entity due to its inherent 4^- charge of the core. We could detect the ions m/z 2140 and 2853 at as low as 100 V (capillary voltage) with clear isotopic resolution. Concentration of the cluster used was 1 $\mu\text{g}/\text{mL}$ to avoid intercluster interactions in the solution as well as in the gas phase. This concentration gave a signal-to-noise ratio of ~ 1000 . These conditions of capillary voltages and concentration used are the lowest for any monolayer protected cluster reported so far.

The presence of a different number of isomers for other charge states shows that isomerism is also charge state

dependent. At similar experimental conditions, two peaks were found in the drift profile of $\text{Ag}_{44}(\text{FTP})_{30}^{3-}$ (m/z 2853) pointing to two isomeric species for this charge state (see [Figure 2](#)). Two spots at 12.2 and 9.7 ms were observed with 84 and 16% relative population. Higher drift time compared to the 4^- charged species is attributed to the lower charge state of the ion. These two peaks gave the same mass spectrum, which were in good agreement with the calculated one.

All of these four isomers (for the 4^- species) show significant differences in their collision cross section (CCS) values. Experimental CCS values are 829.8, 838.4, 872.2, and 896.7 \AA^2 , respectively (see [Table S1](#)). These differences correspond to significantly large structural changes between the isomers. For example, changes in CCS observed for the cis isomers and the all-trans isomer of lycopene were 180 and 236 \AA^2 , respectively, which were separated by Dong et al. using IM MS.¹⁹ A similar experiment on $\text{Au}_{25}(\text{PET})_{18}^-$ showed only one spot in the mobilogram indicating the presence of only one isomer in the experimental condition. This is quite expected from its highly symmetric structure and is similar to the previous report by Dass et al.²⁰ Isomers were not detected for any of the other Au_{25} cluster ions (with other ligands; dodecanethiol, butanethiol) which have been examined ([Figure S3](#)). It has also been confirmed by a study on $\text{Ag}_{25}(\text{DMBT})_{18}$ which again exhibits only one isomer as suggested by the structure ([Figure S4](#)). As all of these clusters have been crystallized and their mass spectra are well-defined in accordance with their molecular structure, we do not believe that the cluster core undergoes a large structural change during ionization. However, in the same process, the monolayer structure can access various conformational states. Such possibilities are larger for clusters having $\text{M}_2(\text{SR})_5$ staples than with $\text{M}_2(\text{SR})_3$ staples. Looking carefully, $\text{Ag}_{44}(\text{SR})_{30}$ possesses an unusual structure. It has a two-shell Keplerate metal core protected by six $\text{Ag}_2(\text{SR})_5$ units. The first hollow 12

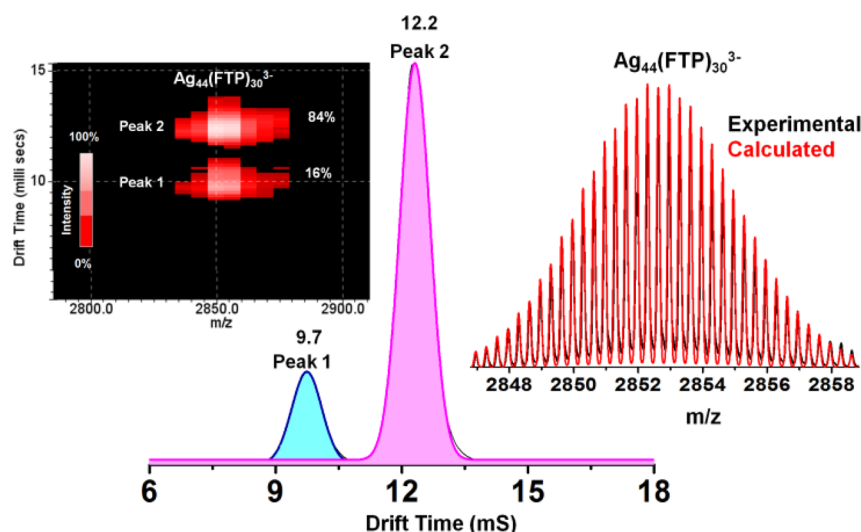


Figure 2. Drift time vs m/z plot of $\text{Ag}_{44}(\text{FTP})_{30}^{3-}$ showing the presence of two isomeric structures. The relative abundances of the isomers are 16% and 84%. Corresponding drift profile and mass spectrum are shown in insets (i) and (ii), respectively.

silver atom icosahedral core is protected with another 20 atom dodecahedral metal shell, together having a nearly perfect I_h point group.¹² This implies that a core rearrangement is unlikely during mass spectrometric measurement. However, each $\text{Ag}_2(\text{SR})_5$ unit is connected to one of the edges of Ag_{20} forming a pentagonal dodecahedron through Ag-SR interactions. For an $\text{Ag}_2(\text{SR})_5$ motif, each Ag is connected to two SR units, and there is another bridging SR unit between two Ag atoms of a $\text{Ag}_2(\text{SR})_5$ staple, which could be simplified as $(\text{SR})_2\text{Ag-SR-Ag}(\text{SR})_2$. This unique orientation is not there in any other cluster examined here. As for example, $\text{Au}_{25}(\text{SR})_{18}$ and $\text{Ag}_{25}(\text{SR})_{18}$ have $\text{Au}/\text{Ag}_2(\text{SR})_3$ staples which can be simplified as $\text{SR-Au/Ag-SR-Au/Ag-SR}$. Due to the difference in thiolate staple structure, there are multiple possibilities for the S-R bond orientation in gas phase during mass spectral measurement. Such possibilities for the existence of different conformers on the cluster surface are supported by recent studies of vibrational circular dichroism of clusters.²¹ Ligands play a major role in deciding the structure of monolayer protected clusters. It is worth noting that the metal surfaces can become chiral through adsorption of molecules though they are symmetric as a whole. This can also be true in the case of metal particles and clusters as well. In the case of $\text{Au}_{38}(\text{SCH}_2\text{CH}_2\text{Ph})_{24}$, for example, the chirality of the molecule arises from the chiral arrangement of the ligands on the cluster surface.²² The bare cluster core has D_{3h} symmetry with a slight distortion, which is lowered by the protecting staples to give the D_3 point group. The chiral arrangement of the staples induces chirality to the cluster system.^{21,23} Recently, a pair of structural isomers of $\text{Au}_{38}(\text{SCH}_2\text{CH}_2\text{Ph})_{24}$ cluster was discovered by Tian et al., by the modification of the synthetic protocol.²² One of these isomers has a core-shell structure with a face-fused bi-icosahedral Au_{23} core, capped by a second shell of remaining 15 gold atoms. Whereas, the other isomer has a Au_{23} core composed of one icosahedral Au_{13} core and one Au_{10} unit and the mixed surface layer consists of two $\text{Au}_3(\text{SR})_4$ staple units, three $\text{Au}_2(\text{SR})_3$ staple units, three $\text{Au}_1(\text{SR})_2$ staple units, and one bridging thiolate SR ligand.²² Another cluster, $\text{Au}_{28}(\text{SR})_{20}$, also shows ligand induced isomerism as revealed by its crystal structure.²⁴

The isomeric forms shown by ion mobility studies may be arising as a result of gas phase dissociation dynamics of the cluster ions. In the solid state, however, all of the clusters exhibit only one isomer as revealed by their crystal structures. Such ion dynamics of the cluster ions happening in the mass spectrometric time scale of a few microseconds are difficult to be studied by all electron calculations.^{25,26}

In order to obtain insights into the isomeric structures, DFT calculations (please see the [Methods](#) section and the [Supporting Information](#)) were performed on $\text{Ag}_{44}(4\text{-FTP})_{30}^{4-}$. Changes in the $\text{Ag}_2(4\text{-FTP})_5$ staple structures were considered as the reason for the origin of the isomeric structures. $[\text{Ag}_{44}(4\text{-FTP})_{30}]^{4-}$ was modeled based on the crystal structure of $[\text{Ag}_{44}(\text{SR})_{30}]^{4-}$. In it FTP ligands bonded to the core of the cluster were replaced with $-\text{SMe}$ to reduce the computational cost. Note that, we have computed only $[\text{Ag}_{44}(4\text{-FTP})_6(\text{SCH}_3)_{24}]^{4-}$ in its most stable ionic form, and the rest of the discussion in this section is based on this ion. The new staples may be considered as $-(\text{MeS})_2-\text{Ag}-(4\text{-FTP})-\text{Ag}-(\text{SMe})_2$. In $[\text{Ag}_{44}(4\text{-FTP})_6(\text{SCH}_3)_{24}]^{4-}$, 4-FTP ligands were acting as bridges by connecting two S-Ag-S staples. As the bridging sulfur is not directly attached to any of the core Ag atoms, we assumed that opening of staples at this position would require less energy and would have least effect on the core and, therefore, the overall geometry. In order to get the structures with opened staples, one Ag-S-Ag staple was opened and the FTP ligand was kept away from the S-Ag-S unit, and this structure was optimized using the DFT method. The structure of the core was not disturbed due to the breaking of one staple bond, but the optimized S-Ag-S angle changes from 112° to 165° in the detached state (labeled as 1). The calculated S-Ag-S angle is related to the Ag atom detached from the staple. The angle changes from 112° (crystal structure) to 165° (staple opened structure in the gas phase). This variation indicates the reorganization of the structure due to the opening of the staple. This change causes an increase in the total energy of the cluster when compared to the closed structure. We observed the reformation of staples during the optimization of structures containing two and three opened staples. This signifies that more staple opened structures are least stable and may not be formed in the experimental

conditions. The energetic instability of geometries than the closed structure and the absence of appropriate environment for the 4-FTP ligands to facilitate π - π stacking in the staple opened form are likely to be the reasons for this. To calculate the energetics of more than one staple opened structures, the distance between S of 4-FTP and Ag (from the detached S–Ag–S), after bond scission was fixed at 6 Å, which is the same as in 1. Four possible isomeric structures computed are shown in Figure 3 (and Figure S5) where one and two staples alone

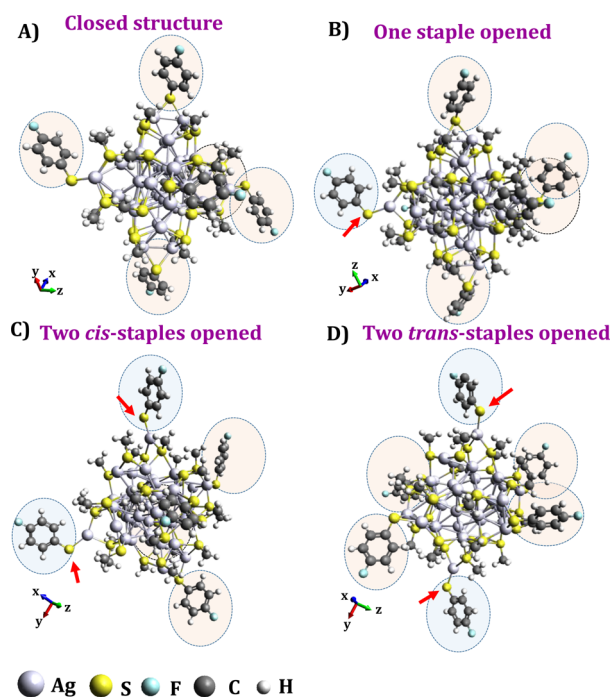


Figure 3. DFT optimized structures of different isomers of $[\text{Ag}_{44}(\text{SMe})_{24}(\text{4-FTP})_6]^{4-}$. Optimized geometries of (A) intact, (B) one staple opened (1), (C) two cis-staples opened, and (D) two trans-staples opened structures. Six axial ligands were optimized without any geometrical constraints. The other 24 positions were replaced with –SMe. Six 4-FTP ligands are circled. Opened positions are shown with arrows and are differently colored.

are opened. Two staple opened structures can result in cis and trans isomers. Staple opened structures are less stable than the closed structures. The relative energies for all staple-opened-geometries were calculated with respect to the closed geometry, which follow the order closed (0 kcal/mol) < one staple opened (8.74 kcal/mol) < two cis-staples opened (18.54 kcal/mol) < two trans-staples opened (20.13 kcal/mol) < three staples opened (28.63 kcal/mol). Opening of staples leads to the reduction in overlap between the orbitals of silver and sulfur atoms, and it affects the energies of molecular orbitals. Consequently, the HOMO–LUMO gap of isomeric structures is different from the structure with closed staples. The calculated HOMO–LUMO energy gaps are given in Table S4. They decrease with the increase in the number of opened staples. Hence, the optical and reactivity properties of these isomers could be different. The relative sizes of the ions also follow a similar trend as calculated, without considering the effect of all of the actual ligands (4-FTP). Each staple opening increases the effective CCS value. Therefore, the isomer with the least CCS value is the intact structure without any staple opening. This can be seen from the Gaussian form of the peak

without any shoulder peaks or much broadening. The next intense peak at drift time 9.8 ms may be due to one staple-opened structure. Other two less intense peaks may be due to two cis- and trans-opened structures. As with more staple opening, the structure may become distorted and will not be spherical in nature; hence, there might be a difference between the experimentally obtained CCS values with the calculated ones. As the structures were not optimized with all of the real ligands, it is difficult to make one-to-one correspondence among the experimentally obtained isomers with the calculated structures. Inclusion of all of the 4-FTP ligands may change the energy and the overall size of the geometries, and the trend could be slightly different.

A change in structure can also arise during desolvation of the charged droplet. The degree of droplet evaporation is dependent on the viscosity and surface tension of the solvent used. $\text{Ag}_{44}(\text{FTP})_{30}$ is soluble in dimethylformamide (DMF), dichloromethane (DCM), and acetonitrile (ACN), and the viscosity of the solvents follow the order DMF (0.92 mPa s) > DCM (0.43 mPa s) > ACN (0.34 mPa s), all at 298 K. Surface tensions of ACN, DCM, and DMF are 29.29, 26.50, and 37.10 mN/m, respectively. For the 4^- charge state, we could separate all of the four isomers when DCM was used as the solvent. In contrast, only two isomers could be resolved for the same charge state when the other two solvents were used (Figure S6). It appears that solvents with moderate surface tension and viscosity can reveal more structural information in such cluster systems.

Monolayer induced isomerism in clusters was further confirmed from measurements of $\text{Ag}_{44}(p\text{-MBA})_{30}$. The 4^- and 3^- ions exhibit different number of isomers like in the case of $\text{Ag}_{44}(\text{FTP})_{30}$. While the 4^- state of $\text{Ag}_{44}(p\text{-MBA})_{30}$ shows three isomers (Figure 4A–C), the 3^- state shows five isomers (Figure 4D–F). These are likely to be due to the various degrees of hydrogen bonding among the carboxyl groups of the *p*-MBA ligands, coupled with the ligand conformations at the surface. These isomers are closely similar in size and shape as seen by the very small difference in their drift times. Effective CCS values for three isomers in the case of $\text{Ag}_{44}(p\text{-MBA})_{30}^{4-}$ are 819.1, 854.2, and 882.7 Å², respectively (see Table S2). A similar study on the $\text{Ag}_{44}(\text{DFTP})_{30}$ cluster showed two isomers as shown in Figure S7 for the 4^- charged species. The effective CCSs for these two isomers are 862.4 and 889.4 Å², respectively (see Table S3). These data further prove that the isomers observed are ligand induced.

We may speculate that isomeric structures of the ions may arise due to the electronic instabilities such as Jahn–Teller distortion. $\text{Ag}_{44}(\text{SR})_{30}$ shows three prominent charge states (4^- , 3^- , and 2^-) in ESI MS, irrespective of the ligand. It is known that the core possesses inherent 4^- charge, which is reflected in the highest intense peak in the mass spectral analysis. The charge can be redistributed between the core and the ligand shell during mass analysis, which can cause drifting of electron density from the highest occupied molecular orbital and lead to structural instability in the system. However, the phenomenon of isomers is not specific to open shell structures, and we do not observe isomers exclusively for them. Therefore, we suggest that the isomers are likely to be derived from ligand conformations as shown above. The observed isomeric structures are distinctly different from co-ordination isomerism seen during ligand exchange.²⁷ This latter variety arises from the many possibilities a ligand experiences upon substitution at various sites. Such isomers are seen when mixed ligands exist in

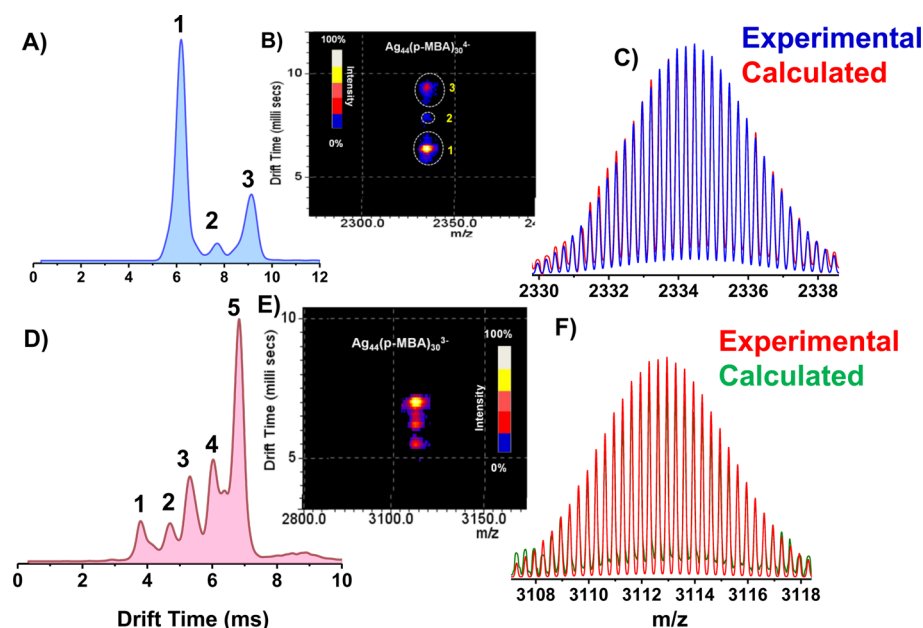


Figure 4. (A) Drift time profile of $\text{Ag}_{44}(\text{MBA})_{30}^{4-}$ three peaks indicating isomeric structures. Corresponding m/z vs drift time vs m/z plot is shown in B. (C) Isotope distribution of peak 1 is in exact agreement with the calculated pattern. (D) Similar study on $\text{Ag}_{44}(\text{MBA})_{30}^{3-}$ showing 5 major peaks in the drift profile. Corresponding m/z vs drift time plot is shown in (E). Mass spectrum of peak 5 is shown in (F) which matches with the calculated isotope pattern. Minor differences in the intensities compared to the calculated spectra on either side of the spectrum are due to overlapping peaks.

a cluster, but the present isomeric structures are arising from clusters composed of only one ligand system.

Similar ligand dependent isomerism is also seen for $\text{Ag}_{29}(\text{BDT})_{12}^{3-}$ where two distinct peaks are seen in the drift time profile, corresponding to two structural isomers (see Figure 5). The $\text{Ag}_{29}(\text{BDT})_{12}$ cluster possess a completely different type of structure as shown in the crystal structure.¹⁸ Essential data confirming the purity of the sample are shown in Figure S8. Although the presence of bidentate thiol as protecting agent makes this cluster stable, it is possible that ligand(s) on one side of the cluster will open up in solution or

in the gas phase. In this process, the total mass of the species remains the same, but there will be small structural variations, leading to isomeric clusters. This is in agreement with the recently reported dimer of $\text{Au}_{25}(\text{SR})_{18}$ clusters in the gas phase, where the thiolate staples on one side of a cluster open up and join the adjacent cluster to form a dimeric cluster ion.²⁸

4. SUMMARY AND CONCLUSIONS

In conclusion, we report experimental and theoretical studies on the existence of isomers in monolayer protected clusters in the gas phase. While two or more isomers are seen for $\text{Ag}_{44}(\text{SR})_{30}$, only one unique isomer is observed for $\text{Au}_{25}(\text{SR})_{18}$ and $\text{Ag}_{25}(\text{SR})_{18}$. The number and relative abundances of the isomers are decided by the nature of the ligand as well as charge state as shown by specific examples. On the other hand, $\text{Ag}_{29}(\text{BDT})_{12}$ possess two distinct separable isomers. The properties of such isomers and the insights they provide on the chemistry of monolayer-protected clusters will be subjects of a future study. We believe that our findings will be helpful to understand the origin of isomerism in clusters in the condensed phase and such isomeric structures might show differences in chemistry/properties in comparison to the known structures. Ionic and molecular chemistries have several parallels as revealed by mass spectrometric studies on various systems. At this point in time, the science of ligand protected clusters has not expanded enough to point out these similarities.

■ ASSOCIATED CONTENT

Supporting Information

The Supporting Information is available free of charge on the ACS Publications website at DOI: 10.1021/acs.jpcc.7b04559.

Synthesis, computational details, ESI MS and ESI IM-MS of different ligand protected $\text{Ag}_{44}(\text{SR})_{30}$ clusters dissolved in different solvents, ESI IM-MS of $\text{Au}_{25}(\text{PET})_{18}$, $\text{Ag}_{25}(\text{DMBT})_{18}$ clusters, UV-vis absorption spectra of

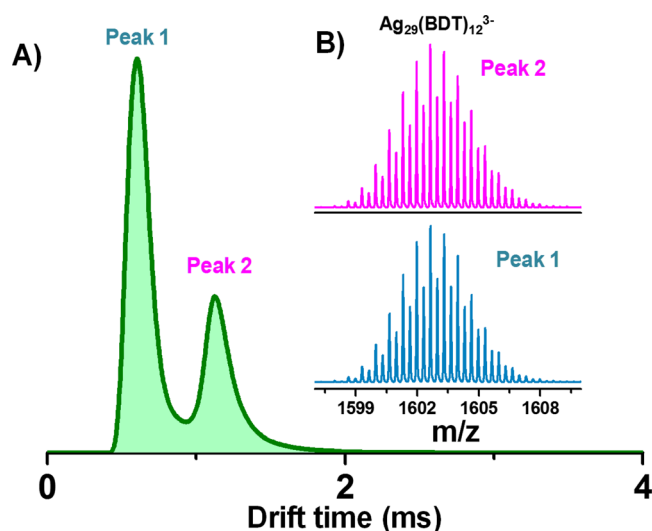


Figure 5. (A) Ion mobility drift time profile of $\text{Ag}_{29}(\text{BDT})_{12}^{3-}$ showing two distinct peaks due to two structural isomers. Both the peaks resulted in similar mass spectra as shown in (B). The two mass spectra match exactly.

different ligand protected $\text{Ag}_{44}(\text{SR})_{30}$ clusters, optimized structure of three staple opened $[\text{Ag}_{44}(\text{FTP})_6(\text{Sme})_{24}]^{4-}$, CCS values of different isomers of $\text{Ag}_{44}(\text{SR})_{30}$, and HOMO–LUMO gap of different isomers of $[\text{Ag}_{44}(\text{SMe})_{24}(4\text{-FTP})_6]^{4-}$. (PDF)

AUTHOR INFORMATION

Corresponding Author

*E-mail: pradeep@iitm.ac.in.

ORCID

Venkatesan Subramanian: 0000-0003-2463-545X

Thalappil Pradeep: 0000-0003-3174-534X

Author Contributions

§A.B. and A.G. have contributed equally to this work.

Notes

The authors declare no competing financial interest.

ACKNOWLEDGMENTS

We thank the Department of Science and Technology, Government of India for continuous support our of research program on nanomaterials. A.B. thanks Dr. Ganapati Natarajan for useful discussions.

REFERENCES

- (1) Natarajan, G.; Mathew, A.; Negishi, Y.; Whetten, R. L.; Pradeep, T. A Unified Framework for Understanding the Structure and Modifications of Atomically Precise Monolayer Protected Gold Clusters. *J. Phys. Chem. C* **2015**, *119*, 27768–27785.
- (2) Lu, Y.; Chen, W. Sub-nanometre sized metal clusters: from synthetic challenges to the unique property discoveries. *Chem. Soc. Rev.* **2012**, *41*, 3594–3623.
- (3) Zhou, M.; Dagan, S.; Wysocki, V. H. Protein subunits released by surface collisions of noncovalent complexes: Nativelike compact structures revealed by ion mobility mass spectrometry. *Angew. Chem., Int. Ed.* **2012**, *51*, 4336–4339.
- (4) Zhou, M.; Huang, C.; Wysocki, V. H. Surface-Induced Dissociation of Ion Mobility-Separated Noncovalent Complexes in a Quadrupole/Time-of-Flight Mass Spectrometer. *Anal. Chem.* **2012**, *84*, 6016–6023.
- (5) Zhou, M.; Wysocki, V. H. Surface Induced Dissociation: Dissecting Noncovalent Protein Complexes in the Gas phase. *Acc. Chem. Res.* **2014**, *47*, 1010–1018.
- (6) Harkness, K. M.; Balinski, A.; McLean, J. A.; Cliffel, D. E. Nanoscale Phase Segregation of Mixed Thiolates on Gold Nanoparticles. *Angew. Chem., Int. Ed.* **2011**, *50*, 10554–10559.
- (7) Harkness, K. M.; Cliffel, D. E.; McLean, J. A. Characterization of thiolate-protected gold nanoparticles by mass spectrometry. *Analyst* **2010**, *135*, 868–874.
- (8) Harkness, K. M.; Fenn, L. S.; Cliffel, D. E.; McLean, J. A. Surface Fragmentation of Complexes from Thiolate Protected Gold Nanoparticles by Ion Mobility-Mass Spectrometry. *Anal. Chem.* **2010**, *82*, 3061–3066.
- (9) Harkness, K. M.; Hixson, B. C.; Fenn, L. S.; Turner, B. N.; Rape, A. C.; Simpson, C. A.; Huffman, B. J.; Okoli, T. C.; McLean, J. A.; Cliffel, D. E. A Structural Mass Spectrometry Strategy for the Relative Quantitation of Ligands on Mixed Monolayer-Protected Gold Nanoparticles. *Anal. Chem.* **2010**, *82*, 9268–9274.
- (10) Baksi, A.; Harvey, S. R.; Natarajan, G.; Wysocki, V. H.; Pradeep, T. Possible isomers in ligand protected Ag_{11} cluster ions identified by ion mobility mass spectrometry and fragmented by surface induced dissociation. *Chem. Commun.* **2016**, *52*, 3805–3808.
- (11) Desireddy, A.; Conn, B. E.; Guo, J.; Yoon, B.; Barnett, R. N.; Monahan, B. M.; Kirschbaum, K.; Griffith, W. P.; Whetten, R. L.; Landman, U.; Bigioni, T. P. Ultrastable silver nanoparticles. *Nature* **2013**, *501*, 399–402.

(12) Yang, H.; Wang, Y.; Huang, H.; Gell, L.; Lehtovaara, L.; Malola, S.; Häkkinen, H.; Zheng, N. All-thiol-stabilized Ag_{44} and $\text{Au}_{12}\text{Ag}_{32}$ nanoparticles with single-crystal structures. *Nat. Commun.* **2013**, *4*, 10.1038/ncomms3422

(13) Yang, H.; Wang, Y.; Yan, J.; Chen, X.; Zhang, X.; Hakkinen, H.; Zheng, N. Structural Evolution of Atomically Precise Thiolated Bimetallic $[\text{Au}_{12+n}\text{Cu}_{32}(\text{SR})_{30+n}]_4$ ($n = 0, 2, 4, 6$) Nanoclusters. *J. Am. Chem. Soc.* **2014**, *136*, 7197–7200.

(14) Yoon, B.; Luedtke, W. D.; Barnett, R. N.; Gao, J.; Desireddy, A.; Conn, B. E.; Bigioni, T.; Landman, U. Hydrogen-bonded structure and mechanical chiral response of a silver nanoparticle superlattice. *Nat. Mater.* **2014**, *13*, 807–811.

(15) Joshi, C. P.; Bootharaju, M. S.; Alhilaly, M. J.; Bakr, O. M. $[\text{Ag}_{25}(\text{SR})_{18}]^+$: The “Golden” Silver Nanoparticle. *J. Am. Chem. Soc.* **2015**, *137*, 11578–11581.

(16) Heaven, M. W.; Dass, A.; White, P. S.; Holt, K. M.; Murray, R. W. Crystal Structure of the Gold Nanoparticle $[\text{N}(\text{C}_8\text{H}_{17})_4][\text{Au}_{25}(\text{SCH}_2\text{CH}_2\text{Ph})_{18}]$. *J. Am. Chem. Soc.* **2008**, *130*, 3754–3755.

(17) Zhu, M.; Aikens, C. M.; Hollander, F. J.; Schatz, G. C.; Jin, R. Correlating the Crystal Structure of A Thiol-Protected Au_{25} Cluster and Optical Properties. *J. Am. Chem. Soc.* **2008**, *130*, 5883–5885.

(18) AbdulHalim, L. G.; Bootharaju, M. S.; Tang, Q.; Del Gobbo, S.; AbdulHalim, R. G.; Eddaoudi, M.; Jiang, D.-e.; Bakr, O. M. $\text{Ag}_{29}(\text{BDT})_{12}(\text{TPP})_4$: A Tetravalent Nanocluster. *J. Am. Chem. Soc.* **2015**, *137*, 11970–11975.

(19) Dong, L.; Shion, H.; Davis, R. G.; Terry-Penak, B.; Castro-Perez, J.; van Breemen, R. B. Collision Cross-Section Determination and Tandem Mass Spectrometric Analysis of Isomeric Carotenoids Using Electrospray Ion Mobility Time-of-Flight Mass Spectrometry. *Anal. Chem. (Washington, DC, U. S.)* **2010**, *82*, 9014–9021.

(20) Angel, L. A.; Majors, L. T.; Dharmaratne, A. C.; Dass, A. Ion Mobility Mass Spectrometry of $\text{Au}_{25}(\text{SCH}_2\text{CH}_2\text{Ph})_{18}$ Nanoclusters. *ACS Nano* **2010**, *4*, 4691–4700.

(21) Dolamic, I.; Varnholt, B.; Burgi, T. Chirality transfer from gold nanocluster to adsorbate evidenced by vibrational circular dichroism. *Nat. Commun.* **2015**, *6*, 7117.

(22) Tian, S.; Li, Y.-Z.; Li, M.-B.; Yuan, J.; Yang, J.; Wu, Z.; Jin, R. Structural isomerism in gold nanoparticles revealed by X-ray crystallography. *Nat. Commun.* **2015**, *6*, 10012.

(23) Dolamic, I.; Knoppe, S.; Dass, A.; Burgi, T. First enantioseparation and circular dichroism spectra of Au_{38} clusters protected by achiral ligands. *Nat. Commun.* **2012**, *3*, 798.

(24) Chen, Y.; Liu, C.; Tang, Q.; Zeng, C.; Higaki, T.; Das, A.; Jiang, D.-e.; Rosi, N. L.; Jin, R. Isomerism in $\text{Au}_{28}(\text{SR})_{20}$ Nanocluster and Stable Structures. *J. Am. Chem. Soc.* **2016**, *138*, 1482–1485.

(25) Ojanperae, A.; Havu, V.; Lehtovaara, L.; Puska, M. Nonadiabatic Ehrenfest molecular dynamics within the projector augmented-wave method. *J. Chem. Phys.* **2012**, *136*, 144103.

(26) Doltsinis, N. L.; Marx, D. First principles molecular dynamics involving excited states and nonadiabatic transitions. *J. Theor. Comput. Chem.* **2002**, *1*, 319–349.

(27) Niihori, Y.; Kikuchi, Y.; Kato, A.; Matsuzaki, M.; Negishi, Y. Understanding Ligand-Exchange Reactions on Thiolate-Protected Gold Clusters by Probing Isomer Distributions Using Reversed-Phase High-Performance Liquid Chromatography. *ACS Nano* **2015**, *9*, 9347–9356.

(28) Baksi, A.; Chakraborty, P.; Bhat, S.; Natarajan, G.; Pradeep, T. $[\text{Au}_{25}(\text{SR})_{18}]_2^{2+}$: A noble metal cluster dimer in the gas phase. *Chem. Commun.* **2016**, *52*, 8397–8400.